CHEMMEDCHEM

DOI: 10.1002/cmdc.200800320

C6-Unsubstituted Pyrazolo[3,4-*d*]pyrimidines Are Dual Src/Abl Inhibitors Effective against Imatinib Mesylate Resistant Chronic Myeloid Leukemia Cell Lines

Maria Alessandra Santucci,[b] Valentina Corradi,[c] Manuela Mancini,[b] Fabrizio Manetti,[c] Marco Radi,[c] Silvia Schenone,*[a] and Maurizio Botta[c]

*Docking simulations were used to predict the most favorable interaction between the T315I mutated form of Abl (invariably associated with resistance to the tyrosine kinase inhibitor imatinib mesylate, IM) and C6-unsubstituted and substituted pyrazolo[3,4-d]pyrimidines previously found to be dual Src/Abl inhibitors. Two C6-unsubstituted (**1** and **2**) and eight C6-substituted compounds (**3**–**10**) were selected and assayed for their effects on the Ba/F3 cell line transducing the wild-type p210Bcr–Abl construct, which is IM-sensitive, or three of the most common mutations associated with IM resistance in vivo (T315I, Y253F, and E255K), and driven to drug resistance by saturating doses of IL-3 or by the expression of the Bcr–Abl construct coding for the p185 protein of acute lymphoblastic leukemia. Compounds **1** and **2** were active against all cell lines assayed (LD_{50} range: 0.7–4.3 μM), whereas C6-substituted compounds exhibited lower activity (LD_{50} ~ 8 μM for compound **3** toward the T315I mutant). Notably, **1** and **2** were also effective toward the T315I mutation, which is insensitive to dual Src/Abl inhibitors. The cytotoxic effects of **1** and **2** on IM-sensitive and IM-resistant Ba/F3 cells were attributable, at least in part, to their pro-apoptotic activity. Taken together, such findings suggest that C6-unsubstituted pyrazolo[3,4-d]pyrimidines may represent useful inhibitors to target IM-resistant chronic myeloid leukemia.*

Introduction

The Bcr–Abl fusion gene, resulting from the juxtaposition of the c-Abl proto-oncogene on chromosome 9 to Bcr sequences on chromosome 22, is the causative event of chronic myeloid leukemia (CML).[1] The transforming capacity of its p210 kDa protein (p210Bcr–Abl) arises from the constitutive activation of the Abl tyrosine kinase (TK), promoting proliferation and survival of leukemic progenitors through interactions with multiple downstream pathways.[2] The TK inhibitor imatinib mesylate (IM, formerly referred to as STI571 or Gleevec) stabilizes p210Bcr–Abl in a catalytically inactive conformation and achieves durable responses in most CML patients. Consequently, it is presently considered the standard therapy for CML. However, the emergence of drug resistance in more than half of patients in the accelerated or blastic phase and approximately 16% of patients in the chronic phase dampened the initial enthusiasm.[3] Bcr–Abl point mutations are the most frequent cause of IM resistance. They preclude drug binding to the Abl catalytic domain by either direct steric hindrance or destabilization of its inactive conformation.[4] Therefore, the development of drugs targeting p210Bcr–Abl TK in the open or active conformation is the major challenge in CML therapy.[5] The high sequence homology between Src and Abl kinases and the structural similarity of their active conformations, combined with the putative role of Src (not inhibited by IM) in the outcome of an IM-resistant phenotype, led to the suggestion that Src inhibitors could represent useful tools for CML treatment.[6] Preclinical and clinical studies showed that ATP-competitive dual Src/Abl inhibitors BMS-35825 (dasatinib),[7] SKI-606 (bosutinib),[8] INNO 406 (NS-187),[9] AP23464[10] and PD166326[11] inhibit p210Bcr–Abl TK more efficiently than IM and overcome IM resistance caused by most mutations, with the notable exception of T315I. Indeed, T315I has been considered the major frontier in the targeted therapy of CML ever since its identification as the most deleterious mutation, conferring complete resistance to all clinically available TK inhibitors.

So far, the only drugs effective against T315I mutation in vitro and in vivo are the two Aurora kinases inhibitors VX-680[12] and PHA-739358[13,14] and the new inhibitor PPY-A.[15] In addition to Bcr–Abl point mutations, IM resistance may arise from other mechanisms including gene amplification, altered drug transport within the cell, protection by the hematopoietic microenvironment and cytokines, Bcr–Abl downstream pathways and Bcr–Abl-independent events.[16,17] These observations prompt further research towards the development of new

[a] *Prof. S. Schenone*
Dipartimento di Scienze Farmaceutiche
Università degli Studi di Genova
Viale Benedetto XV 3, 16132 Genova (Italy)
Fax: (+39) 010-353-8866

[b] *Dr. M. A. Santucci, Dr. M. Mancini*
Istituto di Ematologia e Oncologia Medica "Lorenzo e Ariosto Seràgnoli"
Università degli Studi di Bologna
Via Massarenti 9, 40138 Bologna (Italy)

[c] *Dr. V. Corradi, Dr. F. Manetti, Dr. M. Radi, Prof. M. Botta*
Dipartimento Farmaco Chimico Tecnologico
Università degli Studi di Siena
Via Alcide de Gasperi 2, 53100 Siena (Italy)

Supporting information for this article is available on the WWW under http://dx.doi.org/10.1002/cmdc.200800320

drugs capable of curing IM-resistant CML and/or preventing the selection of drug-resistant cells under IM therapy. In this context, we have recently identified a class of pyrazolo[3,4-*d*]pyrimidine derivatives acting as dual inhibitors of Src and Abl kinases and promoting apoptotic death of CML cell lines.[18] In an effort to improve their activity, a combination of docking studies and molecular interaction field (MIF) analysis led to the design and synthesis of new analogues with enhanced affinity toward Abl.[19] Herein we describe the application of a computational approach combining molecular dynamics (MD) and simulated annealing (SA) simulations aimed at building a T315I model in the absence of ligand. This, in turn, was used for predicting the affinity of pyrazolo[3,4-*d*]pyrimidine derivatives for the T315I mutated form of Abl. The cytotoxic effects of selected compounds on Bcr–Abl-expressing cell lines either sensitive or resistant to IM, were evaluated. Only the C6-unsubstituted derivatives affected proliferation and survival of Ba/F3 cells expressing the wild-type Bcr–Abl construct (sensitive to IM) or driven to IM resistance by the most common Bcr–Abl mutations associated with IM resistance in vivo (Y253F, E255K and T315I), by autocrine growth factor (namely, IL-3) loop and by expression of the Bcr–Abl construct coding for p185 protein, most frequently associated with CML progression to blast crisis.[20–22]

Results

Construction of a model of the T315I mutant in the absence of ligand

At the time this study started, the crystallographic structure of the T315I Bcr–Abl mutant was not available. As a consequence, a computational approach was applied to build the three-dimensional structure of the T315I mutant starting from the available crystallographic structure of the catalytic domain of Abl in complex with VX-680.[12] The seven possible rotamers of the I315 side chain were built by replacing T315 with isoleucine and were represented on the basis of different theoretical values of $\chi1$ and $\chi2$ dihedral angles, as indicated in Table 1.

To investigate the conformational behavior of the I315 side chain in the absence of ligand and to identify the most representative rotamer of this residue, an approach combining MD simulations and SA studies was carried with Gromacs 3.3 software[23–25] using the GROMOS96 43a1 force field. Analysis of the MD and SA trajectories and I315 side chain behavior were performed using several utilities of the Gromacs package. In particular, the dihedral angle values of the I315 side chain were monitored during the 2 ns MD run (Figure 1 A). A cluster analysis of the different values assumed by $\chi1$ during MD showed that the dihedral angle underwent no significant variation, with an average value of 120.47° in the range 93.88–153.42°. In fact, using cutoff values ranging from 0.1 to 0.01 nm, the clustering algorithm used (single linkage algorithm)[26] assigns all frames to the same cluster. With regard to $\chi2$, two principal clusters were found for a cutoff value of 0.01 nm. The first 139 ps of the simulation form the first cluster, while the remaining 1861 ps constitute the most populated cluster assuming an average values of −112.68°.

Table 1. $\chi1$ and $\chi2$ dihedral angles for the seven rotamers of the I315 side chain.

Rotamer	Theoretical values		Dihedral values after geometry optimization	
	$\chi1$ [°]	$\chi2$ [°]	$\chi1$ [°]	$\chi2$ [°]
rot_1a	180	180	209.8	179.8
rot_1b	180	60	195.6	108.3
rot_1c	180	−60	200.0	−75.1
rot_2a	60	180	75.3	176.1
rot_2b	60	−60	81.7	−92.7
rot_3a	−60	180	−60.0	197.9
rot_3b	−60	−60	−45.6	−60.5

The average values of $\chi1$ and $\chi2$ found during MD simulations were assigned to a T315I mutated structure of Abl which was in turn minimized with the same geometry optimization protocol previously reported for the seven I315 rotamers and compared with them. The resulting $\chi1$ and $\chi2$ values correspond to the rotamer indicated as rot_2b in Table 1.

In a second step, a SA protocol was used as a tool to sample the conformational space of the I315 side chain in the active site. This method is based on the similarity between locating the global minimum of the potential energy function of a molecule and the slow cooling required to obtain a perfect crystal.[27] Application of this concept to the exploration of the conformational space can be translated in terms of starting the simulation at a sufficiently high temperature to overcome energy barriers to allow exploration of different regions of the conformational space, and then decreasing the temperature gradually until the system is frozen at the global minimum. In this case, to determine if the rotamer identified from MD calculations is the most favorable for T315I Bcr–Abl in the absence of ligand, a constrained SA investigation was carried out. During SA runs, position restraints were defined for the whole protein with the exception of I315, allowing this residue to reach low-energy conformations. As a result, values of $\chi1$ dihedral angle ranged between 100.68° and 136.55° with an average value of 120.97°. Exactly as in MD simulation, a cluster analysis of values assumed by $\chi1$ during SA cycles groups the frames in the same cluster, whereas cluster analysis for the $\chi2$ values shows three clusters (cutoff value of 0.02 nm). After the initial steps, this dihedral stabilized forming the most populated cluster with an average value of −95.82°. Average values of $\chi1$ and $\chi2$ dihedral angles found with the SA protocol are very similar to those derived from the MD simulation, indicating that the conformational space of the I315 side chain was well explored and reached convergence in the SA calculation as well as convergence with the MD results (Figure 1 B).

As a consequence of these findings, the two approaches taken with the aim to investigate the most probable conformation of the T315I side chain in the absence of ligand showed very similar results, and allowed us to use rot_2b as the reference structure for docking studies.

Two crystallographic structures of T315I Abl were recently published with the new T315I inhibitor PPY-A bound (Protein

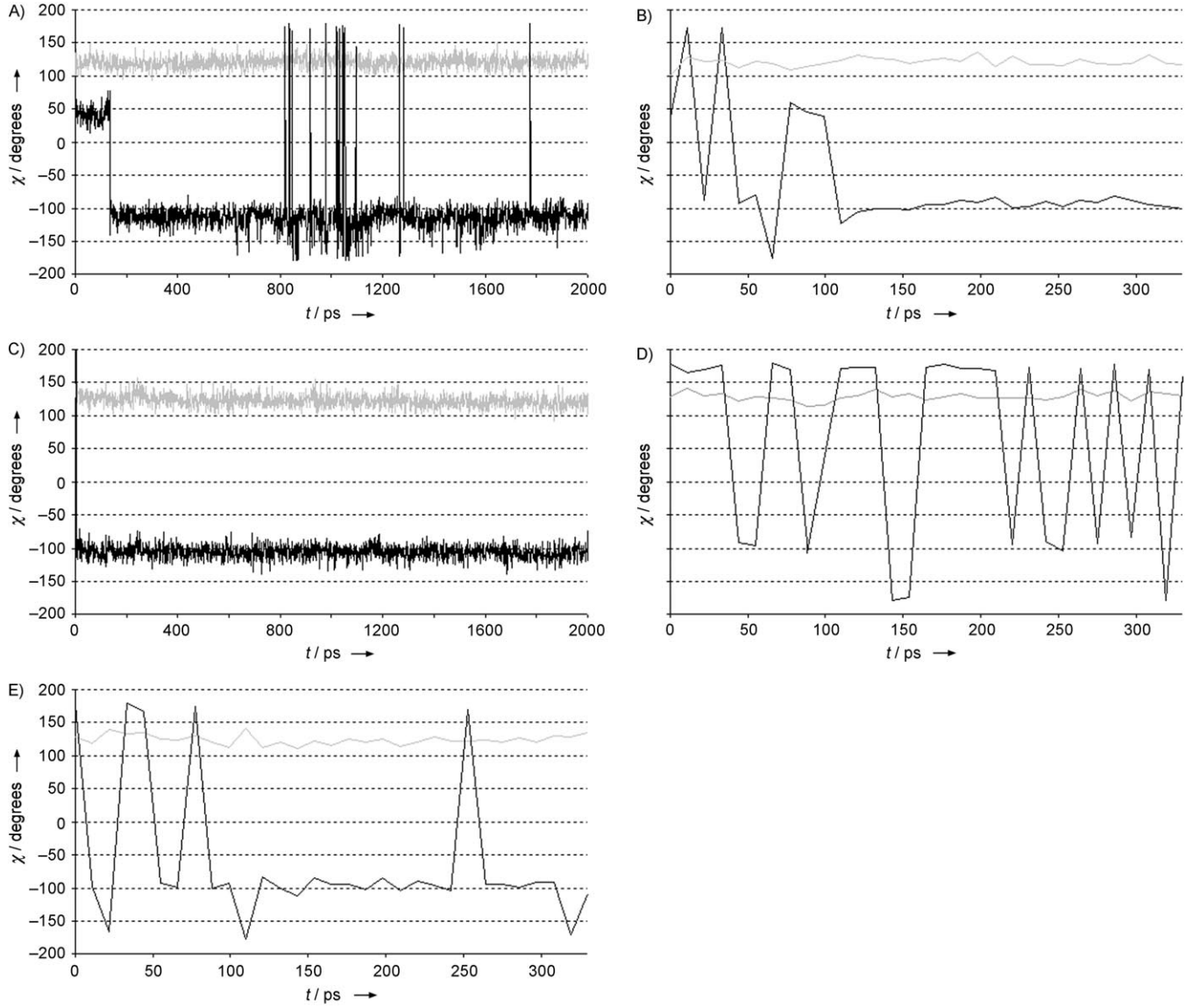

Figure 1. Values of $\chi1$ (gray line) and $\chi2$ (black line) dihedral angles of the I315 side chain. A), B): Time profiles of $\chi1$ and $\chi2$ during A) MD simulations and B) SA cycles on a model built from the PDB 2F4J structure by replacing T315 with an isoleucine residue. C)–E) Evolution of $\chi1$ and $\chi2$ as a function of C) MD run and D) SA cycles for the PDB 2Z60 structure after ligand removal, and E) SA cycles applied to the PDB 2Z60 structure allowing a major relaxation of protein structure.

Data Bank entry 2Z60)[15] and with the Aurora kinase inhibitor PHA-739358 bound (PDB entry 2V7A)[28]. The I315 side chain of these structures adopts a different conformation with respect to our results. However, it should be taken into account that our T315I model was built in the absence of ligand. As a consequence, the model itself is not affected by any structural rearrangement induced by interactions with a ligand. To analyze the behavior of the crystallographic I315 without ligand influence, the above mentioned computational procedures were applied to the 2Z60 structure after ligand removal. During MD simulation (Figure 1C), the $\chi1$ and $\chi2$ dihedrals quickly stabilize to average values very similar to those found in our previous studies (Figure 1A). SA applied to the 2Z60 structure shows, in this case, a fluctuation between two possible average $\chi2$ values of 173.22° and −93.00° (Figure 1D). Superposition of C-α of 2Z60 and rot_2b revealed a root mean square deviation (rmsd) value of 0.458 Å. Furthermore, small differences in side chain orientations near I315 (i.e., L370, D381, E286, V256) can be identified and related to the presence of the ligand PPY-A in the crystallographic structure, affecting, in that way, the $\chi2$ dihedral conformation. For these reasons, SA calculations were applied to the 2Z60 structure without position restraints for I315 and also for other residues near the gatekeeper position (L370, I314, E317, V299, A269). In this case, allowing a less restrained relaxation of the protein structure, the $\chi1$ and $\chi2$ dihedrals of I315 can stabilize more easily to values close to those found with our model (Figure 1E). These results suggest that the rotamer rot_2b chosen as the structure for docking calculations was a reliable starting point.

Docking studies on the T315I Abl model discriminate C6-unsubstituted pyrazolo[3,4-*d*]pyrimidines from C6-substituted analogues

The protein model built for the T315I mutant was used to analyze the binding mode of a large set of pyrazolo[3,4-*d*]pyrimidines. The reliability of the molecular docking protocol was initially checked by simulating the orientation and interactions of VX-680 within the binding site of PDB entry 2F4J[12] and comparing the results with the crystallographic structure. For this purpose, the ligand was removed and a geometry optimization of the protein structure was performed (energy minimization) to avoid possible steric clashes affecting the X-ray structure. Then, the ligand structure taken out from the protein underwent random translations and rotations. Next, the software GOLD, version 3.0.1,[29–31] was employed to perform docking simulations of the VX-680 ligand within the active site of the relaxed protein structure. The best-ranking structure of this simulation belongs to the most populated cluster and was compared with experimental data. The orientation and conformation predicted by the program are very similar to the crystallographic structure and the hydrophobic and hydrogen bond interactions of VX-680 binding were reproduced. Because VX-680 is effective against wild-type and T315I Bcr–Abl forms, docking studies of this compound were performed using Gold to verify if the interactions between VX-680 and the binding site with T315 are also maintained in the mutant form. The four hydrogen bonds described for VX-680 in the H396P enzyme[12] are also reproduced in our mutant model with the docked compound and the same hydrophobic regions are occupied, suggesting the computational protocol as a reliable tool to investigate the binding mode of Abl inhibitors.

Docking results for pyrazolo[3,4-*d*]pyrimidines showed that C6-unsubstituted derivatives had the same pattern of profitable interactions already found in the complexes with the wild-type Abl,[18] while C6-alkylthio analogues did not reproduce this binding mode. Based on the modeling predictions, two C6-unsubstituted derivatives already tested in cell-free assays against wild-type enzyme (Table 2) were selected for biological studies on Bcr–Abl mutants. In particular, **1** represents the parent compound of derivatives bearing two aromatic substituents at positions 1 and 4 of the pyrazolo[3,4-*d*]pyrimidine nucleus, while **2** was very recently synthesized on the basis of a structure-based ligand optimization approach aimed at developing more active compounds.[19] Finally, different compounds belonging to the C6-substituted class of derivatives (compounds **3**–**10** in Table 2) were also selected on the basis of available enzymatic activity against wild-type Abl enzyme, to check the reliability of the molecular modeling predictions.

Pyrazolo[3,4-*d*]pyrimidines 1 and 2 inhibit the activating phosphorylation of Bcr–Abl, Src, and Lyn kinases

We first investigated the inhibitory effects of pyrazolo[3,4-*d*]pyrimidines **1** and **2** on their specific targets Bcr–Abl, Src and downstream Lyn kinases in parental and either IM-sensitive or IM-resistant Bcr–Abl-transducing Ba/F3 cells. The drug-resistant phenotype resulted from: 1) three of the most common Bcr–Abl mutations associated with IM resistance in vivo (Y253F, E255K, and T315I), 2) IL-3 receptor saturating concentrations (provided by 10% WEHI-3 conditioned medium as the source of IL-3), and 3) expression of a Bcr–Abl construct coding for the alternative 185-kDa protein of acute lymphoblastic leukemia (ALL), frequently associated with CML progression to blast crisis.[20–22] In preliminary experiments, the response of all the

Table 2. General structure, enzymatic affinity toward Abl, and Ba/F3 cytotoxic effects of pyrazolo[3,4-*d*]pyrimidines.

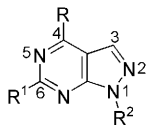

Compd	R	R^1	$R^{2[a]}$	K_i [μM][b]	LD_{50} [μM][c]					
					Parental	p210Bcr–Abl				p185Bcr–Abl
						wt	Y253F	E255K	T315I	+IL-3	
1	$NHCH_2C_6H_5$	H	A	0.40±0.06	0.5±0.1	4.4±0.1	4.3±0.2	3.3±0.2	3.5±0.3	1.9±0.1	1.5±0.2
2	$NHCH_2C_6H_4$-*p*F	H	B	0.08±0.04	0.8±0.1	2.7±0.1	3.2±0.2	2.5±0.4	3.0±0.3	0.70±0.05	1.5±0.2
3	$NHCH_2C_6H_5$	SCH_3	A	0.30±0.10	ND[d]	8.1±0.3	>10	5.5±0.3	7.9±0.3	>10	7.4±0.3
4	NHC_6H_4-*m*Cl	SCH_3	A	0.60±0.10	ND[d]	>10	>10	>10	>10	>10	>10
5	$NHCH_2C_6H_4$-*o*Cl	SCH_3	A	0.09±0.02	ND[d]	>10	>10	>10	>10	>10	>10
6	NHC_6H_4-*m*Br	SCH_3	A	0.06±0.02	ND[d]	>10	>10	>10	>10	>10	>10
7	NHC_4H_9	SCH_2CH_3	A	0.32±0.10	ND[d]	>10	>10	>10	>10	>10	>10
8	$NHCH_2C_6H_5$	S-cyclopentyl	A	0.06±0.02	ND[d]	>10	>10	>10	>10	>10	>10
9	$NHCH_2CH_2C_6H_5$	S-cyclopentyl	A	0.07±0.02	ND[d]	>10	>10	>10	>10	>10	>10
10	$NHCH_2C_6H_5$	SCH_2CH_2-(4-morpholino)	A	0.09±0.02	ND[d]	>10	>10	>10	>10	>10	>10

[a] A = 2-chloro-2-phenylethyl, B = 2-chloro-2-(4-chlorophenyl)ethyl. [b] K_i values toward Abl were calculated as reported in ref. [19] for compounds **1**–**2**, and in ref. [18] for compounds **3**–**10**. [c] Lethal dose 50 values toward parental Ba/F3 cells, Ba/F3 cells expressing wild-type Bcr–Abl (wt), Ba/F3 cells expressing Y253F, E255K, and T315I mutations associated with IM resistance, Ba/F3 cells grown in the presence of 10% WEHI-3 as source of IL-3 and Ba/F3 cells expressing the Bcr–Abl coding for p185. Results are the mean values of three repeat experiments. Standard errors did not exceed 10%. [d] Not determined.

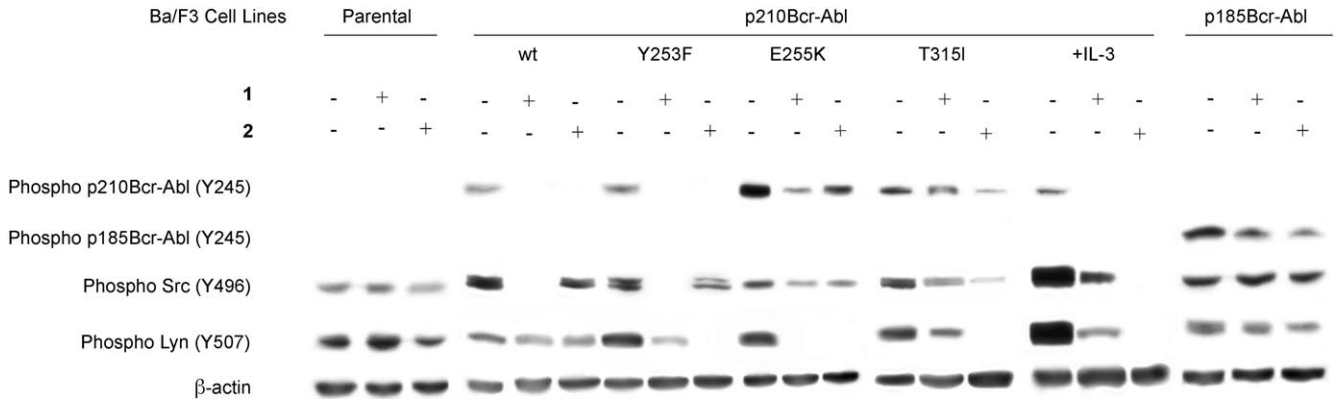

Figure 2. Expression levels and phosphorylation status of proteins involved in the response of Bcr–Abl-expressing cells to pyrazolo[3,4-*d*]pyrimidines **1** and **2**. Protein expression was evaluated by means of immunoprecipitation (IP)/immunoblotting analysis in whole-cell lysates. Cell types were evaluated for protein expression levels and phosphorylation status at 48 h treatment with **1** and **2** at a concentration of 5 μM. Densitometric analysis was used to determine statistical significance of differences in signal intensities. Results were confirmed in two additional replicates (wt = wild-type).

above mentioned cell types to IM was evaluated (Supporting Information, figure S4). In particular, the Y253F mutation was confirmed to confer an intermediate resistance to IM, while the E255F and T315I mutations confer high resistance to IM.[32] The number of Bcr–Abl transcript molecules in IM-sensitive and IM-resistant Ba/F3 cells, assayed by means of a previously published competitive PCR strategy,[33] did not exhibit a significant difference (ranging from $1.20\times10^7\pm0.2\times10^6$ to $1.38\times10^7\pm0.4\times10^6$), supporting the hypothesis that drug resistance did not arise from the fusion gene amplification. Moreover, cells resistant to IM as a consequence of IL-3 did not develop or select mutations in the Abl TK domain, supporting previously published results found in Bcr–Abl-expressing 32D cells.[22]

Figure 2 shows that **1** and **2** completely inhibit p210Bcr–Abl phosphorylation at Y245 (at the SH2 linker domain, conditional upon Y425 phosphorylation at the activation loop) in Ba/F3 cells expressing wild-type Bcr–Abl and Y253F mutation, and in Ba/F3 cells resistant to IM in consequence of IL-3 addition to the culture media. Moreover, **1** and **2** significantly decreased Y245 p210Bcr–Abl phosphorylation in Ba/F3 cells expressing E255K and T315I mutations. A similar result was found for the phosphorylation of Y245 on p185Bcr–Abl. In addition, they significantly decreased Src phosphorylation at Y496 and Lyn phosphorylation at Y507 in all the cell types, with the exception of those expressing p185Bcr–Abl. The impact of the two compounds on Src and Lyn kinase phosphorylation in individual cell types was quite similar. Notably, Lyn hyperphosphorylation was observed in all IM-resistant cell types, supporting its participation in the development of a drug-resistant phenotype.[34]

Cytotoxic effects of pyrazolo[3,4-*d*]pyrimidines on IM-sensitive and IM-resistant Ba/F3 cells

Cell response to C6-unsubstituted and C6-substituted pyrazolo[3,4-*d*]pyrimidines was evaluated in clonogenic assays (0.9% methylcellulose), and lethal dose 50 (LD_{50}) values were calculated by dedicated software (GraphPad Software, Inc.). Compounds **1** and **2** exhibited cytotoxic effects against both IM-sensitive and IM-resistant cells. Ba/F3 cells expressing the wild-type Bcr–Abl, Y253F and E255K mutations (which are sensitive to dual Src/Abl inhibitors BMS-35825, SKI-606, INNO-406, PD166326 and AP23464)[9,10,35–37] were significantly sensitive to both compounds, whose LD_{50} ranged between 2.5 and 4.4 μM (Table 2). Notably, **1** and **2** were active against T315I mutation (LD_{50} 3.5 and 3.0 μM, respectively), which is highly resistant to IM and to all the above mentioned dual Src/Abl inhibitors. This result was in agreement with computational simulations predicting **1** and **2** to have high affinity for T315I Abl. Furthermore, they were also active against Ba/F3 cells driven to IM resistance by saturating IL-3 concentrations and by p185Bcr–Abl expression. The last result led to the suggestion that **1** and **2** could be a useful tool for the treatment of CML where the drug-resistant phenotype was promoted by other events than fusion gene mutations and in CML blast crisis. Furthermore, both compounds significantly decreased parental Ba/F3 cell clonogenic activity. Further studies on myeloid progenitors from CML patients and normal controls are required to confirm the lack of specificity of **1** and **2** against leukemic cells. Notably, their cytotoxicity on parental Ba/F3 cells is similar to that reported for VX-680.[15] Compounds bearing a thio substituent at the C6 position of the pyrazolo-pyrimidine scaffold exhibited a very low cytotoxic activity against IM-sensitive (expressing the wild-type Bcr–Abl) and all the IM-resistant Ba/F3 cells. The concentration required to decrease cell clonogenic activity to 50% or less was in all cases higher than 10 μM, with the exception of **3**, for which lower LD_{50} values were observed (Table 2).

The cytotoxicity of **1** and **2** on IM-sensitive and IM-resistant Bcr–Abl-expressing Ba/F3 cells arises, at least in part, from their pro-apoptotic effects. In fact, 48 h exposure of IM-sensitive and IM-resistant Ba/F3 cells to each of the two compounds at 5 μM induced apoptotic death (Figure 3).

Discussion and Conclusions

In spite of the outstanding results of IM in the treatment of CML, much interest is directed toward the development of new and more effective drugs capable of curing or preventing

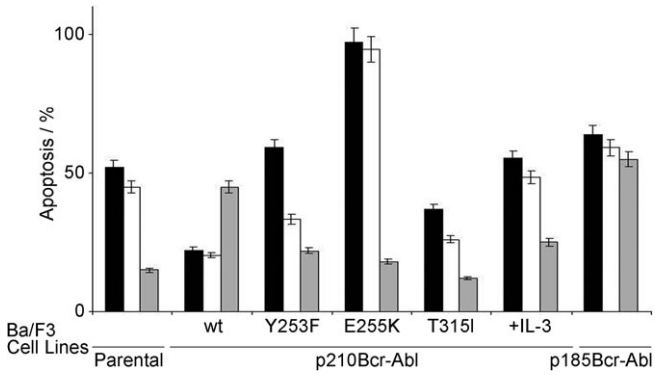

Figure 3. Cell death induction in response to compounds **1**, **2**, and IM. Cells were assayed for apoptosis induction in response to **1** (black), **2** (white) and IM (gray) by means of cytofluorimetric analysis of annexin V and PI uptake. Untreated cells displayed apoptotic cell death levels lower than 5%. Results are expressed as apoptotic cell percentage at 48 h exposure to 5 μM **1**, **2**, and IM. Results are the mean values of three repeated experiments ±SE.

the outcome of drug resistance.[38,39] IM resistance is more often associated with CML accelerated phase and blast crisis, and almost invariably occurs in Philadelphia+ ALL expressing p185Bcr–Abl. In the chronic phase, it mostly arises from Bcr–Abl mutations at the Abl TK domain which directly impair drug binding (T315I, F317L and F359V) or prevent conformational changes required for IM binding, either in the P-loop (M244V, G250E, Q252H/R, Y253F/H) or near the activation loop (E255K). Alternatively, it may proceed from Bcr–Abl amplification or Bcr–Abl-independent mechanisms, including depletion of IM intracellular levels by enhanced drug efflux or multidrug-resistance (MDR1) gene overexpression and activation of Bcr–Abl downstream signaling pathways.[17,40] The high structural homology of Src and Abl in their active conformation and the crucial role of Src kinase (not inhibited by IM) in the outcome of IM-resistant phenotype led to the advance of dual Src/Abl inhibitors for CML treatment.[6] Indeed, some ATP-competitive inhibitors of Bcr–Abl and Src kinases, including BMS-35825 (dasatinib), SKI-606 (bosutinib), INNO-406 (NS-187), AP23464, and PD166326 have greater inhibitory activity toward p210Bcr–Abl relative to IM and the ability to overcome IM resistance caused by most mutations, with the notable exception of T315I.[13]

We have recently identified a family of dual Src/Abl inhibitors with a pyrazolo[3,4-*d*]pyrimidine scaffold that decrease proliferation and direct Bcr–Abl-positive cell lines toward apoptotic death.[18,19] At the time this study started, the crystallographic structure of the T315I Bcr–Abl mutant was not available. As a consequence, a three-dimensional model of the structure of the T315I mutant was built starting from the available crystallographic structure of the Abl catalytic domain in complex with the Aurora kinase inhibitor VX-680 (PDB entry 2F4J).[12] The T315 residue of such a structure was replaced with isoleucine, and the seven possible rotamers of its side chain were built. Next, a combined approach of MD and SA calculations was applied to investigate the effects induced by T315I mutation on the structure of Abl in the absence of ligand and to find the best conformational model of T315I Abl to be used for subsequent docking calculations.

Results from docking of pyrazolo[3,4-*d*]pyrimidines on T315I Abl showed that the C6-unsubstituted derivatives display a more favorable pattern of interactions with the protein than those found for the C6-substituted analogues. In particular, the unsubstituted compounds were characterized by an interaction pathway similar to that previously found in the active site of wild-type Abl.[18] In fact, the pyrazolopyrimidine nucleus of **1** and **2** is located in the region usually occupied by the adenine ring of ATP, allowing the usual hydrogen bond motif between M318 and the pyrimidine core (Figure 4A and 4B). The amino group at C4 and the N5 atom of the ligand form hydrogen bonds with the carbonyl oxygen and the backbone NH group of M318, respectively, while important hydrophobic contacts occur with the hydrophobic region I (V256, K271, M290, V299, I313) and II (L248, G249, G321). On the other hand, C6-substituted pyrazolo[3,4-*d*]pyrimidines could not retrieve their typical binding mode found for the wild-type Abl active site, where the backbone carbonyl group of M318 is involved in a hydrogen bond with the C4 amino group of the inhibitor.[18] In fact, in the T315I Abl active site, **3**, probably because of the steric hindrance of the isoleucine residue, revealed a flipped binding mode characterized by the loss of the fundamental hydrogen bond with M318, while hydrophobic interactions with the hydrophobic regions I and II were maintained (Figure 4C). Superposition of **1** and **2** with VX-680 (Figure 4D) shows the correspondence between the C4 amino group of pyrazolopyrimidines and the C4 amino group on the pyrimidine core of VX-680. Moreover, the pyrimidine core of **1** and **2** matches the methylpyrazole group of VX-680, while the N1 phenyl ring of the pyrazolopyrimidines is accommodated into the same hydrophobic region (namely, the hydrophobic region I) of the cyclopropyl substituent of VX-680.

Two crystallographic structures of T315I Abl were recently published: PDB entries 2Z60[15] and 2V7A,[28] bound to the inhibitors PPY-A and PHA-739358, respectively. The I315 side chain of these structures adopts a different conformation relative to our model. However, it should be noted that our T315I model was built in the absence of ligand and, consequently, is not affected by any structural rearrangement induced by interactions with a ligand. Despite the difference with the crystallographic structure, the reliability of our T315I model was supported by applying the same protocol to the 2Z60 structure and by docking **1**–**3** in its binding site (further details available in Supporting Information).

Compounds **1**–**10** were selected to evaluate their activity and cytotoxic effects on relevant targets. Compounds **1** and **2** were selected among the C6-unsubstituted derivatives, while C6-substituted analogues **3**–**10** were chosen to further validate the computational predictions. Immunoprecipitation (IP)/immunoblotting analyses and enzymatic assays in cell-free systems confirmed that **1** and **2** effectively inhibit their enzymatic targets (Figure 2, Table 2). In particular, they completely inhibited p210Bcr–Abl phosphorylation at Y245 in Ba/F3 cells expressing the wild-type Bcr–Abl construct and Y253F mutation and Ba/F3 cells resistant to IM in consequence of IL-3 saturating concentrations. The same compounds significantly decreased p210Bcr–Abl phosphorylation at Y245 in Ba/F3 cells

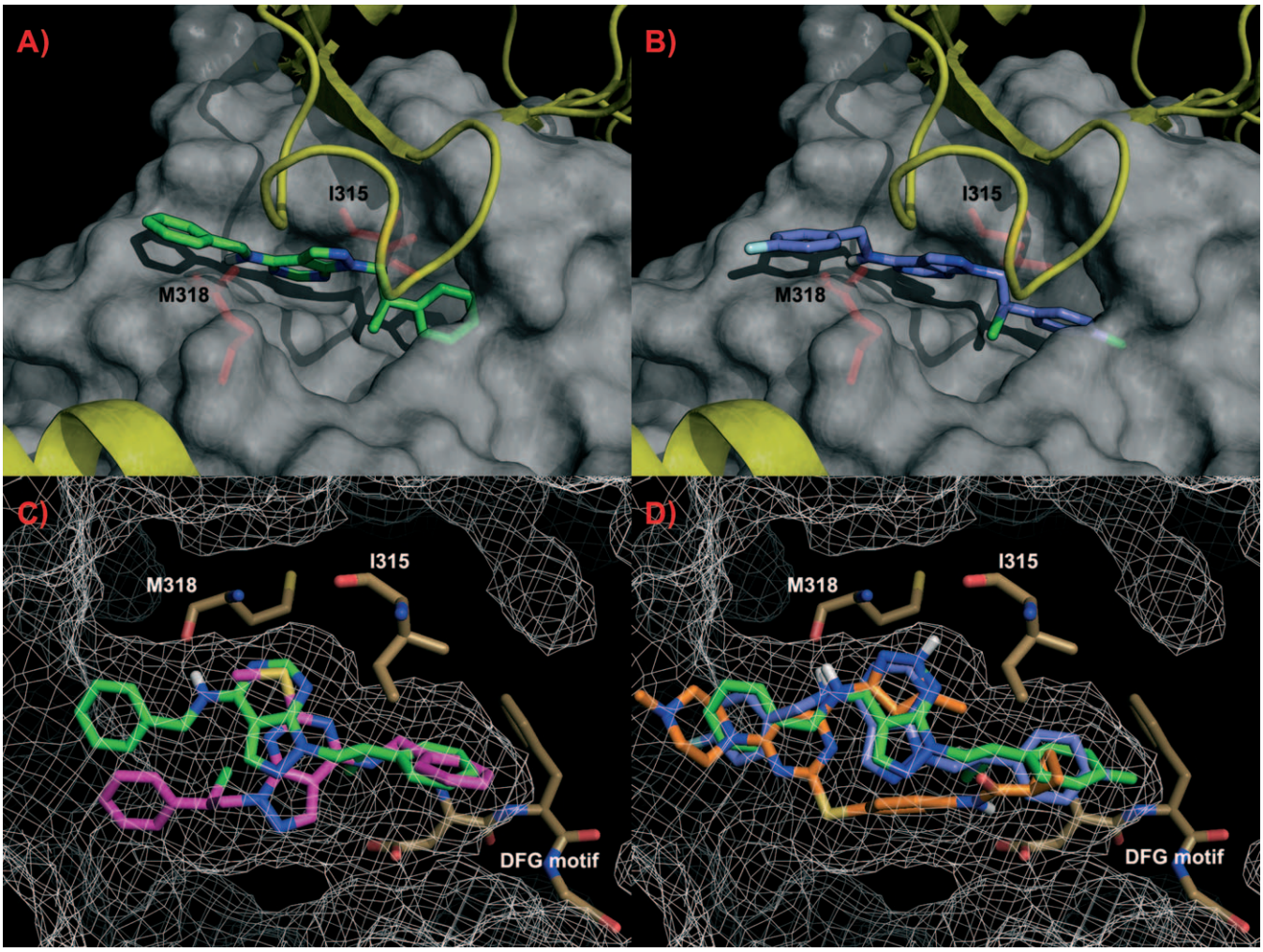

Figure 4. Interactions of pyrazolo[3,4-*d*]pyrimidine derivatives with the ATP binding site of the T315I mutant form of the Abl kinase domain. A) Compound **1** (in green) and B) compound **2** (slate) docked in the T315I model; M318 and I315 are shown in red transparent stick representation. C) Superposition of **1** (green) and **3** (magenta) resulting from docking with the T315I model. D) Compounds **1** (green) and **2** (slate) superimposed with VX-680 (orange); M318, I315, and residues of the DFG motif are shown in light brown.

expressing E255K and T315I mutations and the p185Bcr–Abl construct. In a similar way, they significantly decreased phosphorylation of Src at Y416 and Lyn at Y507 in all the cell types, except the one expressing p185Bcr–Abl (Figure 2). Discrete differences in inhibitory effects of both compounds on Src and Lyn phosphorylation in different cell types were not elucidated. Interestingly, Lyn hyperphosphorylation was apparent in all IM-resistant cell types (Figure 2), confirming its participation in the development of a drug-resistant phenotype suggested by a previous study.[34] Inhibition of p210Bcr–Abl and downstream Src kinases led **1** and **2** to have cytotoxic effects on either IM-sensitive or IM-resistant Bcr–Abl-expressing Ba/F3 cells. Notably, both compounds effectively decreased proliferation and survival of cells expressing the T315I mutation, which do not respond to other dual Src/Abl inhibitors.[13] Moreover, compounds were also active on the alternative Bcr–Abl construct coding for p185 protein associated with Philadelphia+ ALL and lymphoid blast crisis of CML.

A recent study ascribed the drug resistance associated with p185Bcr–Abl expression to microenvironment protective signals, rather than to the fusion protein TK activity or its downstream targets. This hypothesis is further supported by the fact that the drug resistance associated with p185Bcr–Abl expression is extended to TK inhibitor AMN107 (nilotinib), farnesyl transferase inhibitor SCH66336 and CK2 inhibitor K25, in addition to IM.[21,41–43] However, cytotoxic effects of **1** and **2** on Ba/F3 cells expressing p185Bcr–Abl were due to the fusion protein inhibition rather than Src and Lyn inhibition (Figure 2).

In summary, docking studies on T315I Bcr–Abl mutant suggest that only C6-unsubstituted pyrazolo[3,4-*d*]pyrimidines engage the Abl kinase domain in such a way to avoid clashes with gatekeeper residue. As expected, **1** and **2** are effective at micromolar concentrations on p210Bcr–Abl-expressing Ba/F3 cell lines either sensitive or resistant to IM. In particular, they affect proliferation and survival of cells with the T315I mutation, which do not respond to dual Src/Abl inhibitors.

The findings reported herein confirm the better activity profile of C6-unsubstituted compounds[18] over C6-substituted analogues, and highlight a possible role for these compounds in the design of new Bcr–Abl inhibitors of resistance emergence and, in particular, against the deleterious mutation T315I at the gatekeeper position. Further work on hematopoietic progenitors from CML patients and from healthy people is required to confirm the effects of pyrazolo[3,4-*d*]pyrimidine derivatives on normal hematopoiesis.

Experimental Section

Computer modeling

T315I starting structure. The T315I mutated protein model used in docking experiments was built starting from the crystallographic structure of Abl kinase in complex with VX-680, otherwise referred to as MK 0457 (PDB entry 2F4J).[12] The seven possible rotamers of the I315 side chain were built by replacing T315 with an isoleucine residue and were represented on the basis of different theoretical values of $\chi1$ and $\chi2$ dihedral angles, as indicated in Table 1. Finally, for each rotamer, geometry optimization was performed with Polak–Ribiere conjugated gradient method (0.01 kJ mol^{-1} Å convergence) and a continuum solvation method, with water as the solvent, was also applied.

MD simulations. The protein structure with I315 side chain corresponding to rot_1a was chosen as starting structure for MD simulations. The protein was embedded in a box containing SPC water model, with a margin of 1.5 Å between the protein and box edges. Eleven sodium ions were then added to the system in random positions to neutralize the protein's net charge. Internal bad contacts were removed by energy minimization with position restraints for all the heavy atoms of the protein and then without any restraint, using the Steepest Descent algorithm. Energy minimization tolerance was set to 250 kJ mol^{-1} nm^{-1}. After the energy minimization, an MD equilibration run was performed under position restraints for 250 ps allowing the soaking of water molecules of the system. A 2 ns MD run was then performed after the equilibration without constraint and collecting snapshots every 1 ps. The simulation was run under NPT conditions with a reference pressure of 1 bar and reference temperature of 310 K.

SA simulations. The structure resulting from the soaking procedure described above was the starting point for 30 cycles of SA. Each SA cycle was performed including an initial heating stage in which the molecule is heated at 1000 K for 3 ps. The system was then cooled to 700 K for 1.5 ps and to 200 K for 3.5 ps. Next, the protein was kept at 200 K for an additional 3 ps before the next cycle. Altogether, every SA cycle was 11 ps long. Position restraints were applied during SA to the whole system except for I315 to allow the adaptation of the side chain of this residue within the active site. Snapshots were collected every 11 ps, at the end of each SA cycle.

Analysis of the MD and SA trajectories and I315 side chain behavior were performed using several utilities of GROMACS package, such as g_rms, g_rmsf, g_angle, g_chi, g_dist, g_cluster.

Docking studies. The structure of inhibitors was generated using MacroModel 8.5[44] and minimized with OPLSA_2005 force field using the Polak–Ribiere conjugate gradient method and a convergence of 0.001 kJ mol^{-1} Å. Docking studies were performed by means of GOLD software, version 3.0.1[29–31] as previously described.[18] The stability of interactions between protein and inhibitors was confirmed with 1 ns MD simulations, using the protocol described in Supporting Information.

Biological assays

Enzyme assays. Recombinant human Abl was purchased from Upstate Biotechnology (Waltham, MA, USA) and used to investigate the mechanism of kinase inhibition, as previously reported.[18,19]

Cell lines and treatments. Ba/F3 cells expressing the wild-type Bcr–Abl and T315I, Y253F and E255K mutations were kindly provided by M. W. Deininger (Center for Hematologic Malignancies, Oregon Health and Science University, Portland, OR, USA). Details on site-directed mutagenesis used to generate IM-resistant Bcr–Abl constructs were provided previously.[35] Ba/F3 parental cell line and that expressing the Bcr–Abl construct coding for the 185-kDa p185 protein were donated by R. A. Van Etten (Molecular Oncology Research Institute and Division of Hematology/Oncology, Tufts–New England Medical Center, Boston, MA, USA). Cells were maintained in RPMI supplemented with 10% fetal calf serum (FCS) (Gibco-BRL, Invitrogen, Carlsbad, CA, USA), 10% WEHI-3 conditioned medium as source of IL-3 when required and antibiotics in 5% CO_2 and fully humidified atmosphere at 37 °C. Apoptosis induction was evaluated after 48 h exposure to 1 μM IM and 5 μM selected pyrazolo[3,4-*d*]pyrimidines. The antiproliferative effects were determined in clonogenic assays (0.9% methylcellulose added with 30% FCS). Dedicated software (GraphPad Software, Inc., San Diego, CA) was used to fit dose-response curves and calculate individual cell type sensitivity to compounds. Apoptotic cells were recognized by cytofluorimetric analysis of fluorescein-labeled annexin V (Hoffmann-La Roche, Basel, Switzerland) and propidium iodide (PI) uptake (Sigma, St. Louis, MO, USA). Cell fluorescence and PI uptake were measured with a FACScan low cytometer (Becton Dickinson, Franklin Lanes, NJ, USA) set at $\lambda_{ex} = 488$ nm, and at $\lambda = 539$ nm (bandpass filter) for fluorescein detection or at $\lambda > 580$ nm for PI detection. Analysis of obtained data was performed using dedicated software from Becton Dickinson.

Protein analysis. Immunoprecipitation (IP)/immunoblotting analysis was performed on whole-cell lysates according to a published method.[22] The effects of tested compounds (at a final concentration of 5 μM) on Abl, Src, and Lyn kinase phosphorylation were investigated at 24 h by labeling IP products with antibodies anti-Abl phosphorylated at Y245, anti-Src phosphorylated at Y416, and anti-Lyn phosphorylated at Y507 (all from Cell Signaling Technology Inc., Danvers, MA, USA). Signal intensities in single blots from three repeated experiments were measured by a GS-700 Imagining densitometer (Bio-Rad Laboratories Inc., Hercules, CA, USA) equipped with dedicated software (Molecular Analist, Bio-Rad).

Acknowledgements

The authors thank "Centro Universitario per l'Informatica e la Telematica" of the University of Siena. Financial support from the University of Bologna, Carisbo Foundation, and Bologna AIL is gratefully acknowledged.

Keywords: chronic myeloid leukemia · enzymes · inhibitors · molecular modeling · pyrazolo[3,4-*d*]pyrimidines

[1] J. Groffen, J. R. Stephenson, N. Heisterkamp, A. de Klein, C. R. Bartram, G. Grosveld, *Cell* **1984**, *36*, 93–99.
[2] M. W. N. Deininger, J. M. Goldman, J. V. Melo, *Blood* **2000**, *96*, 3343–3356.
[3] B. J. Druker, F. Guilhot, S. G. O'Brien, I. Gathmann, H. Kantarjian, N. Gattermann, M. W. Deininger, R. T. Silver, J. M. Goldman, R. M. Stone, F. Cervantes, A. Hochhaus, B. L. Powell, J. L. Gabrilove, P. Rousselot, J. Reiffers, J. J. Cornelisse, T. Hughes, H. Agis, T. Fischer, G. Verhoef, J. Shepherd, G. Saglio, A. Gratwohl, J. L. Nielsen, J. P. Radich, B. Simonsson, K. Taylor, M. Baccarani, C. So, L. Letvak, R. A. Larson, IRIS investigators, *N. Engl. J. Med.* **2006**, *355*, 2408–2417.
[4] M. Azam, R. R. Latek, G. Q. Daley, *Cell* **2003**, *112*, 831–843.
[5] G. Martinelli, S. Soverini, G. Rosti, M. Baccarani, *Leukemia* **2005**, *19*, 1872–1879.
[6] M. A. Meyn III, M. B. Wilson, F. A. Abdi, N. Fahey, A. P. Schiavone, J. Wu, J. M. Hochrein, J. R. Engen, T. E. Smithgall, *J. Biol. Chem.* **2006**, *281*, 30907–30916.
[7] M. R. Burgess, B. J. Skaggs, N. P. Shah, F. Y. Lee, C. L. Sawyers, *Proc. Natl. Acad. Sci. USA* **2005**, *102*, 3395–3400.
[8] J. M. Golas, K. Arndt, C. Etienne, J. Lucas, D. Nardin, J. Gibbons, P. Frost, F. Ye, D. H. Boschelli, F. Boschelli, *Cancer Res.* **2003**, *63*, 375–381.
[9] S. Kimura, H. Naito, H. Segawa, J. Kuroda, T. Yuasa, K. Sato, A. Yokota, Y. Kamitsuji, E. Kawata, E. Ashihara, Y. Nakaya, H. Naruoka, T. Wakayama, K. Nasu, T. Asaki, T. Niwa, K. Hirabayashi, T. Maekawa, *Blood* **2005**, *106*, 3948–3954.
[10] T. O'Hare, R. Pollock, E. P. Stoffregen, J. A. Keats, O. M. Abdullah, E. M. Moseson, V. M. Rivera, H. Tang, C. A. Metcalf III, R. S. Bohacek, Y. Wang, R. Sundaramoorthi, W. C. Shakespeare, D. Dalgarno, T. Clackson, T. K. Sawyer, W. Michael, M. W. Deininger, B. J Druker, *Blood* **2004**, *104*, 2532–2539.
[11] D. R. Huron, M. E. Gorre, A. J. Kraker, C. L. Sawyers, N. Rosen, M. M. Moasser, *Clin. Cancer Res.* **2003**, *9*, 1267–1273.
[12] M. A. Young, N. P. Shah, L. H. Chao, M. Seeliger, Z. V. Milanov, W. H. Biggs III, D. K. Treiber, H. K. Patel, P. P. Zarrinkar, D. J. Lockhart, C. L. Sawyers, J. Kuriyan, *Cancer Res.* **2006**, *66*, 1007–1014.
[13] E. Weisberg, P. W. Manley, S. W. Cowan-Jacob, A. Hochhaus, J. D. Griffin, *Nat. Rev. Cancer* **2007**, *7*, 345–356.
[14] A. Gontarewicz, S. Balabanov, G. Keller, R. Colombo, A. Graziano, E. Presenti, D. Benten, C. Bokemeyer, W. Fiedler, J. Moll, T. H. Brümmendorf, *Blood* **2008**, *111*, 4355–4364.
[15] T. Zhou, L. Parillon, F. Li, Y. Wang, J. Keats, S. Lamore, Q. Xu, W. Shakespeare, D. Dalgarno, X. Zhu, *Chem. Biol. Drug Des.* **2007**, *70*, 171–181.
[16] T. O'Hare, A. S. Corbin, B. J. Druker, *Curr. Opin. Genet. Dev.* **2006**, *16*, 92–99.
[17] J. Wu, F. Meng, H. Lu, L. Kong, W. Bornmann, Z. Peng, M. Talpaz, N. J. Donato, *Blood* **2008**, *111*, 3821–3829.
[18] F. Manetti, A. Pucci, M. Magnani, G. A. Locatelli, C. Brullo, A. Naldini, S. Schenone, G. Maga, F. Carraro, M. Botta, *ChemMedChem* **2007**, *2*, 343–353.
[19] F. Manetti, C. Brullo, C. Tintori, M. Magnani, F. Mosci, B. Chelli, E. Crespan, S. Schenone, A. Naldini, O. Bruno, M. L. Trincavelli, G. Maga, F. Carraro, C. Martini, F. Bondavalli, M. Botta, *J. Med. Chem.* **2008**, *51*, 1252–1259.
[20] E. Jabbour, H. Kantarjian, D. Jones, M. Talpaz, N. Bekele, S. O'Brien, X. Zhou, R. Luthra, G. Garcia-Manero, F. Giles, M. B. Rios, S. Verstovsek, J. Cortes, *Leukemia* **2006**, *20*, 1767–1773.
[21] S. Mishra, B. Zhang, J. M. Cunnick, N. Heisterkamp, J. Groffen, *Cancer Res.* **2006**, *66*, 5387–5393.
[22] M. Mancini, G. Brusa, E. Zuffa, P. Corrado, G. Martinelli, T. Grafone, E. Barbieri, M. A. Santucci, *Leuk. Res.* **2007**, *31*, 979–987.
[23] D. van der Spoel, E. Lindahl, B. Hess, G. Groenhof, A. E. Mark, H. J. C. Berendsen, *J. Comput. Chem.* **2005**, *26*, 1701–1718.
[24] E. Lindahl, B. Hess, D. van der Spoel, *J. Mol. Model.* **2001**, *7*, 306–317.
[25] H. J. C. Berendsen, D. van der Spoel, R. van Drunen, *Comput. Phys. Commun.* **1995**, *91*, 43–56.
[26] D. van der Spoel, E. Lindahl, B. Hess, A. R. van Buuren, E. Apol, P. J. Meulenhoff, D. P. Tieleman, A. L. T. M. Sijbers, K. A. Feenstra, R. van Drunen, H. J. C. Berendsen, **2005**, Gromacs User Manual Version 3.3, http://www.gromacs.org (accessed November 3, 2008).
[27] S. Kirkpatrick, C. D. Gelatt, Jr., M. P. Vecchi, *Science* **1983**, *220*, 671–680.
[28] M. Modugno, E. Casale, C. Soncini, P. Rosettani, R. Colombo, R. Lupi, L. Rusconi, D. Fancelli, P. Carpinelli, A. D. Cameron, A. Isacchi, J. Moll, *Cancer Res.* **2007**, *67*, 7987–7990.
[29] G. Jones, P. Willett, R. C. Glen, *J. Mol. Biol.* **1995**, *245*, 43–53.
[30] G. Jones, P. Willett, R. C. Glen, A. R. Leach, R. Taylor, *J. Mol. Biol.* **1997**, *267*, 727–748.
[31] M. L. Verdonk, J. C. Cole, M. J. Hartshorn, C. W. Murray, R. D. Taylor, *Proteins* **2003**, *52*, 609–623.
[32] S. Roumiantsev, N. P. Shah, M. E. Gorre, J. Nicoll, B. B. Brasher, C. L. Sawyers, R. A. Van Etten, *Proc. Natl. Acad. Sci. USA* **2002**, *99*, 10700–10705.
[33] F. Campanini, M. A. Santucci, L. Pattachini, G. Brusa, M. Piccioli, E. Barbieri, L. Babini, S. Tura, *Haematologica* **2001**, *86*, 167–173.
[34] N. J. Donato, J. Y. Wu, J. Stapley, G. Gallick, H. Lin, R. Arlinghaus, M. Talpaz, *Blood* **2003**, *101*, 690–698.
[35] P. La Rosée, A. S. Corbin, E. P. Stoffregen, M. W. Deininger, B. J. Druker, *Cancer Res.* **2002**, *62*, 7149–7153.
[36] T. O'Hare, D. K. Walters, E. P. Stoffregen, T. Jia, P. W. Manley, J. Mestan, S. W. Cowan-Jacob, F. Y. Lee, M. C. Heinrich, M. W. N. Deininger, B. J. Druker, *Cancer Res.* **2005**, *65*, 4500–4505.
[37] M. Puttini, A. M. L. Coluccia, F. Boschelli, L. Cleris, E. Marchesi, A. Donella-Deana, S. Ahmed, S. Redaelli, R. Piazza, V. Magistroni, F. Andreoni, L. Scapozza, F. Formelli, C. Gambacorti-Passerini, *Cancer Res.* **2006**, *66*, 11314–11322.
[38] J. F. Apperley, *Lancet Oncol.* **2007**, *8*, 1018–1029.
[39] J. F. Apperley, *Lancet Oncol.* **2007**, *8*, 1116–1128.
[40] J. V. Melo, C. Chuah, *Cancer Lett.* **2007**, *249*, 121–132.
[41] S. Mishra, V. Pertz, B. Zhang, P. Kaur, H. Shimada, J. Groffen, Z. Kazimierczuk, L. A. Pinna, N. Heisterkamp, *Leukemia* **2007**, *21*, 178–180.
[42] P. Kaur, N. Feldhahn, B. Zhang, D. Trageser, M. Müschen, V. Pertz, J. Groffen, N. Heisterkamp, *Mol. Cancer* **2007**, *6*, 67.
[43] B. Zhang, J. Groffen, N. Heisterkamp, *Leukemia* **2007**, *21*, 1189–1197.
[44] F. Mohamadi, N. G. J. Richards, W. C. Guida, R. Liskamp, M. Lipton, C. Caufield, G. Chang, T. Hendrickson, W. C. Still, *J. Comput. Chem.* **1990**, *11*, 440–467.

Received: October 1, 2008
Published online on November 27, 2008

